Hindawi Publishing Corporation
Advances in Condensed Matter Physics
Volume 2014, Article ID 735878, 6 pages
http://dx.doi.org/10.1155/2014/735878

Research Article

Structural, Optical, and Compactness Characteristics of Nanocrystalline $CaNb_2O_6$ Synthesized through an Autoigniting Combustion Method

K. C. Mathai,[1] S. Vidya,[2] Annamma John,[2] Sam Solomon,[3] and J. K. Thomas[2]

[1] *Department of Physics, St. Aloysius College, Edathua, Kerala 689573, India*
[2] *Electronic Materials Research Laboratory, Department of Physics, Mar Ivanios College, Thiruvananthapuram, Kerala 695 015, India*
[3] *Department of Physics, St. John's College, Anchal, Kollam District, Kerala 691306, India*

Correspondence should be addressed to J. K. Thomas; jkthomasemrl@yahoo.com

Received 31 May 2013; Revised 5 October 2013; Accepted 5 October 2013; Published 9 January 2014

Academic Editor: R. N. P. Choudhary

Nanoparticles of calcium metaniobate compound are prepared by an autoigniting combustion technique and its structural, optical, and dielectric properties are investigated. The X-ray diffraction, Fourier-transform Raman, and infrared studies reveal that calcium metaniobate possesses phase pure orthorhombic columbite structure with space group of Pbcn. The average particle size of the as-prepared nanoparticles obtained from both the Scherrer formula and transmission electron microscopy is ~37 nm. The optical band gap calculated from Tauc's Plot is 3.25 eV. Photoluminescence studies reveal that Calcium metaniobate can be used as an idealphotoluminarmaterial. The powders are pelletised and sintered at an optimized temperature of 1350°C in a short duration of two hours, yielding a high density. The morphology of the sintered pellet is further examined using scanning electron microscopy. The dielectric constant and loss factor values measured at 5 MHz for a well-sintered Calcium metaniobate pellet are found to be 27.6 and 5.3×10^{-4} respectively, at room temperature.

1. Introduction

Calcium metaniobate ($CaNb_2O_6$) crystallizes with orthorhombic columbite structure in the space group of Pbcn(60) and is a strong source of coherent light which can be useful in applications of holography [1]. $CaNb_2O_6$ crystal possesses a low-symmetry crystal structure and the Ca and Nb cations are at the centre of the octahedra surrounded by six oxygen atoms in the $CaNb_2O_6$ columbite structure. The CaO_6 and NbO_6 octahedra form independent zigzag chains by sharing edges and the chains are connected by sharing corners in the order of CaO_6 chain-NbO_6 chain-NbO_6 chain [2, 3]. $CaNb_2O_6$ has good mechanical, dielectric, and thermal properties like thermal conductivity, specific heat, and thermal coefficient of expansion making it suitable for laser crystal host, substrates for electronic circuits, and so forth [1, 3]. The photocatalytic activity of $CaNb_2O_6$ is studied by a number of researchers and Cho et al. reported its enhanced photocatalytic activity for producing H_2 from pure water under UV irradiation [4–7]. $CaNb_2O_6$ also exhibits strong blue luminescence emission under UV light irradiation at 300 K. $CaNb_2O_6$ also possesses interesting properties, namely, piezoelectricity, pyroelectricity, and electrooptic and nonlinear optical activity [8–11]. The compacted calcium-metaniobate ($CaNb_2O_6$) is a good dielectric material for microwave dielectric applications [12–14]. $CaNb_2O_6$, a subcomponent of the complex perovskite family $A(B'_{1/3}B''_{2/3})O_3$ prepared by the conventional route, has been studied for its microwave dielectric properties [15–17]. Generally, the relative band positions, optical band gaps, and so forth, in niobate compounds, are affected by the characteristic of their crystal structure, octahedral distortion, and the ionic size of cations [7]. The various synthesis techniques employed for the preparation of $CaNb_2O_6$ are conventional solid state route, hydrothermal synthesis, solvothermal process, and sol-gel technique [6, 7, 17, 18].

In the present work, we have synthesized calcium metaniobate ($CaNb_2O_6$) nanopowder using an autoigniting combustion technique, and its structural, optical, and dielectric properties are investigated.

2. Experimental

2.1. Synthesis Procedure. In the present autoigniting combustion synthesis, aqueous solution containing ions of Ca and Nb is prepared by dissolving stoichiometric amount of high purity $Ca(NO_3)_2$ (99%, CDH, India) in double distilled water and $NbCl_5$ (99.9%, Alfa Aesar) in hot oxalic acid. Citric acid was added as a complexing agent maintaining the citric acid to the cation ratio at unity. Amount of citric acid was calculated based on total valence of the oxidizing and the reducing agents for maximum release of energy during combustion [16, 19]. Appropriate amount of urea, as fuel, and nitric acid, as oxidizer, was added to the precursor to obtain a clear viscous solution. The solution which is acidic in nature, containing the precursor mixture, was then heated using a hot plate at ~250°C in a ventilated fume hood. The solution boils on heating and undergoes dehydration accompanied by foam. The foam gets ignited by itself on persistent heating giving voluminous and fluffy product of combustion. Thus the obtained as-prepared powder was taken for further characterizations.

2.2. Characterization Technique. The crystal structure of the prepared particle was determined by X-ray technique using PHILIPS XPERT-PRO diffractometer with nickel filtered CuKα radiation of wavelength 1.5406 Å. The Fourier transform-Raman spectrum was carried out at room temperature in the wave number range 50–1200 cm^{-1} using Bruker-RFS/100S spectrometer at a power level of 150 mW and at a resolution of 4 cm^{-1}. The sample was excited with an Nd:YAG laser lasing at 1064 nm, and the scattered radiations were detected using Ge detector. The infrared (IR) spectra of the sample were recorded in the range 400–4000 cm^{-1} using a Thermo-Nicolet Avatar 370 FTIR Spectrometer using KBr pellet method. Particulate properties of the combustion product were examined using transmission electron microscopy (TEM Hitachi H-600, Japan). The photoluminescence (PL) spectrum of the sample was measured using Flurolog@-3 Spectrofluorometer. The photons from the source were filtered by an excitation spectrometer. The monochromatic radiation was then allowed to fall on the disc samples and the resulting radiation was filtered by an emission spectrometer and then fed to a photomultiplier detector. The optical measurements of the nanopowder were carried out at room temperature using a Cary 100 BIO UV-Vis spectrophotometer in the wavelength range 200–700 nm.

To study the sinterability of the nanoparticles obtained by the present combustion method, the as-prepared $CaNb_2O_6$ nanoparticles were mixed with 5% polyvinyl alcohol and pressed in the form of cylindrical pellet of 12 mm diameter and ~2 mm thickness at a pressure about 350 MPa using a hydraulic press. The sintering temperature of the pellet was optimized at 1350°C for 2 hours after conducting many trials.

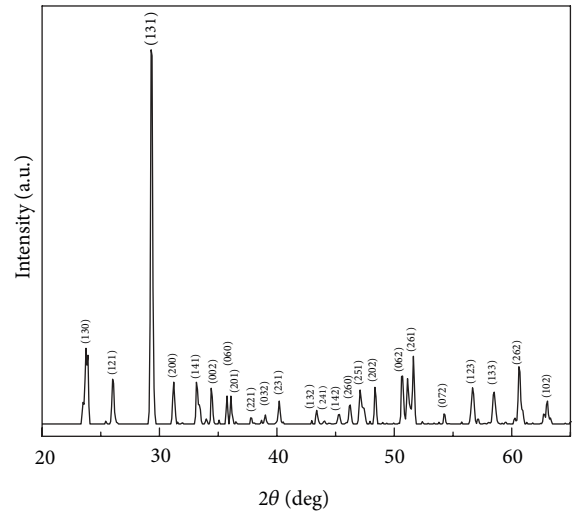

Figure 1: XRD patterns of as-prepared $CaNb_2O_6$.

The surface morphology of the sintered sample was examined using scanning electron microscopy (SEM, Model-JEOL JSM 6390LV). For low frequency dielectric studies the pellet was made in the form of a disc capacitor with the specimen as the dielectric medium. Both the flat surfaces of the sintered pellet were polished and then electroded by applying silver paste. The capacitance of the sample was measured using an LCR meter (Hioki-3532-50LCR HiTester) in the frequency range 100 Hz to 5 MHz at room temperature.

3. Results and Discussion

3.1. Structural Characterizations. Figure 1 shows the XRD patterns of as-prepared calcium metaniobate nanopowder. All the peaks are indexed for orthorhombic structure and agree well with reported value (JCPDS 391392). The calculated lattice constants are $a = 5.727$ Å, $b = 14.807$ Å, and $c = 5.239$ Å, which indicate that the formation of $CaNb_2O_6$ phase is complete during the combustion process itself. The average crystallite size calculated from full width half maximum (FWHM) using the Scherrer formula is ~37 nm.

3.2. FT-Raman and Infrared Spectroscopy of $CaNb_2O_6$. The X-ray diffraction study revealed that the as-prepared nanocrystalline $CaNb_2O_6$ is orthorhombic structure with space group Pbcn. To investigate more on the structural details of $CaNb_2O_6$, FTIR and Raman spectra of the sample are also recorded and are shown in Figures 2 and 3, respectively.

The spectral data of the Raman and IR spectra and the band assignments are given in Table 1. The Raman spectrum over the range 1000–100 cm^{-1} is characterized by the Nb–O stretching vibrations. As expected the $\nu_1(A_g)$ mode which is attributed to the terminal Nb–O stretching vibration is observed as a sharp highly intense band at 904 cm^{-1} [20, 21]. The bridge Nb–O stretching vibration occurs in the range 700–500 cm^{-1} and the chain Nb–O stretching vibration below 500 cm^{-1}. The bands due to ν_2 mode of vibration of

Table 1: Raman and IR spectral data of $CaNb_2O_6$ and their band assignment relative intensities. v: very, s: strong, m: medium, w: weak, sh: shoulder, and br: broad.

Raman (cm^{-1})	Band assignments	IR (cm^{-1})	Band assignments
904 vvs	$\nu_1(A_g)$		
846 w	$\nu_1(B_{1g})$	867 vs	$\nu_1(B_{2u})$
695 vsbr	$\nu_2(A_g)$, $\nu_2(B_{1g})$, $\nu_2(B_{2g})$, $\nu_2(B_{3g})$,	805 s	$\nu_3(B_{1u}) + \nu_7(B_{1u})$
626 sh	$\nu_3(B_{3g})$	747 s	$\nu_2(B_{2u})$
597 vvw	$\nu_3(B_{1g})$		
578 vw	$\nu_6(A_g) + \nu_7(A_g)$/ $\nu_6(B_{2g}) + \nu_7(B_{2g})$		
538 s	$\nu_3(A_g)$	550 vsbr	$\nu_3(B_{1u})$, $\nu_3(B_{2u})$, $\nu_3(B_{3u})$
493 m	$\nu_4(B_{1g})$, $\nu_3(B_{2g})$	497 m	$\nu_4(B_{1u})$, $\nu_4(B_{3u})$
458 vvw	$\nu_4(B_{2g})$		
427 vw	$\nu_5(B_{1g})$		
382 s	$\nu_5(A_g)$, $\nu_5(B_{2g})$		
345 vw	$\nu_7(B_{1g})$		
313 vw	$\nu_6(B_{2g})$		
289 s	$\nu_6(A_g)$, $\nu_7(A_g)$, $\nu_8(B_{1g})$		
262 w	$\nu_9(B_{1g})$, $\nu_7(B_{2g})$		
241 s	$\nu_8(A_g)$		
221 vw	$\nu_9(A_g)$, $\nu_9(B_{2g})$		
194 m	$\nu_{10}(A_g)$		
163 w	$\nu_{12}(B_{1g})$		
136 m	$\nu_{11}(A_g)$, $\nu_{11}(B_{3g})$		
107 vw	$\nu_{12}(B_{2g})$		
75 s	Lattice vibration		

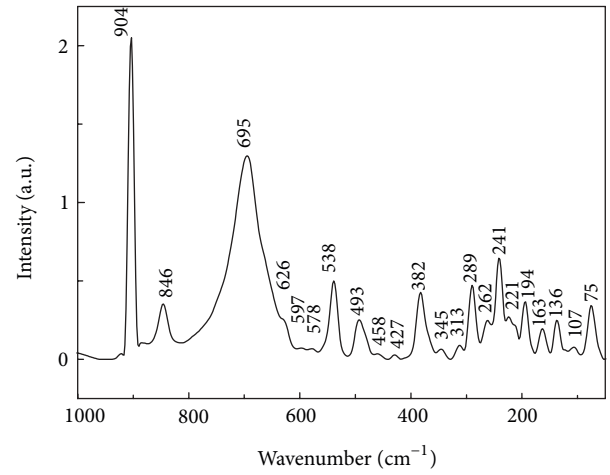

Figure 2: FT-Raman spectrum of the as-prepared $CaNb_2O_6$ nanopowder.

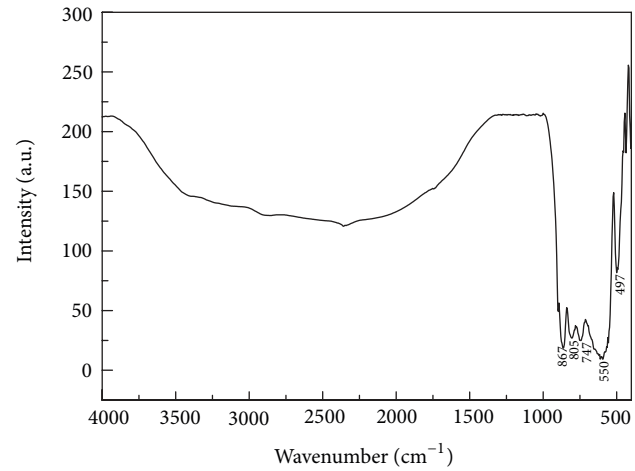

Figure 3: FT-IR spectrum of the as-prepared $CaNb_2O_6$ nanopowder.

the A_g, B_{1g}, B_{2g}, and B_{3g} symmetries appear unresolved and are observed as an intense broad band extending from about 800 to 610 cm^{-1} with the peak at 695 cm^{-1}. The weak band at 578 cm^{-1} may be a combination band due to combination like $\nu_6(A_g) + \nu_7(A_g)$ or $\nu_6(B_{2g}) + \nu_7(B_{2g})$. The O–Nb–O bending vibrations occur in the range 450–100 cm^{-1}. The Ca–O stretching and the vibrations involving the chain bonds and Nb–Nb bonds occur towards the lower wavenumbers of this range. The lowest frequency band at 75 cm^{-1} of appreciable intensity is due to the lattice vibrations.

In the IR-spectrum, intense absorption is observed in the range 900–400 cm^{-1}. The band at 867 cm^{-1} is due to the $\nu_1(B_{2u})$ mode of vibration and that at 747 cm^{-1} is due to the $\nu_2(B_{2u})$ mode. The intense band at 550 cm^{-1} is broadened with shoulders on either side. The broadening may be due to the overlapping of the ν_3 mode of vibration of B_{1u}, B_{2u}, and B_{3u} symmetries. The $\nu_4(B_{1u})$ and $\nu_4(B_{3u})$ modes are observed as a medium intense absorption at 497 cm^{-1}. The band at 805 cm^{-1} may be due to the combination $\nu_3(B_{1u}) + \nu_7(B_{1u})$.

Thus the factors like Nb–O stretching, O–Nb–O bending, Ca–O stretching, and the vibrations involving chain bonds and the broadening of the peaks indicate a slightly distorted (NbO_6 octahedra) crystal structure.

3.3. TEM Studies. TEM image of the $CaNb_2O_6$ samples is shown in Figure 4, and inset shows the corresponding SAED pattern. TEM image of the as-prepared sample showed that the nanoparticles are of submicron size 24–50 nm. The particles are of regular cuboidal shape with average size of nearly 37 nm. The selected area electron diffraction (SAED) pattern indicates the polycrystalline nature of the crystallites. The spotty nature is due to the finer crystallites having related orientations agglomerated together resulting in a limited set of orientations.

3.4. Optical Studies. The UV absorption spectra of the prepared nanoparticles of $CaNb_2O_6$ samples measured using a Cary 100 BIO UV-Vis spectrophotometer in the range 200–700 nm are shown in Figure 5.

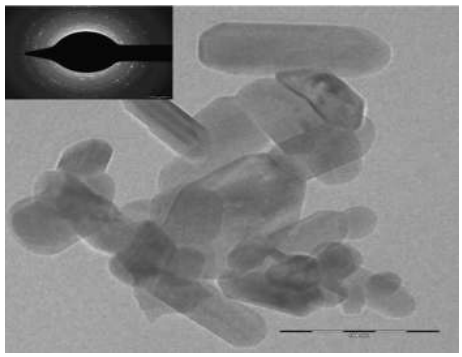

Figure 4: TEM image of as-prepared $CaNb_2O_6$ nanopowder and its SAED pattern inset.

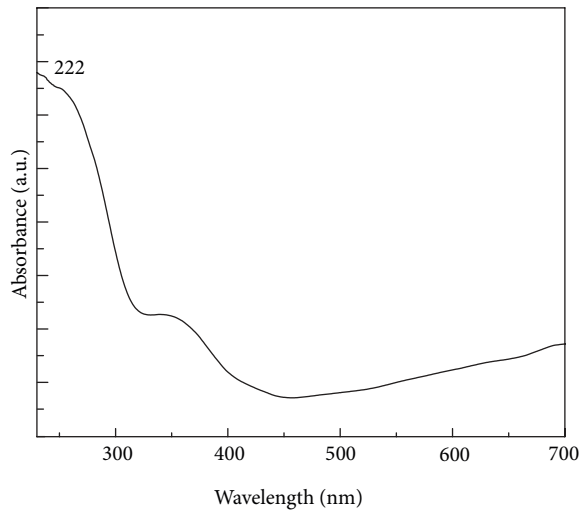

Figure 5: UV-Vis absorption spectrum of $CaNb_2O_6$ nanopowder.

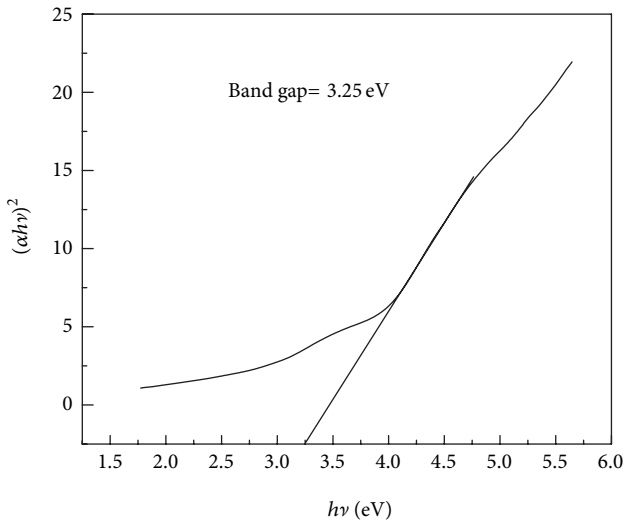

Figure 6: Tauc's plot of the optical absorption spectrum of $CaNb_2O_6$ nanopowder.

In semiconductors, the absorption coefficient near the fundamental edge depends on photon energy. This absorption dependence on photon energy is expressed by Tauc's equation [10]. According to Tauc's relation, the absorption coefficient, for direct band gap material, is given by

$$(\alpha h\nu) = B\left[h\nu - E_g\right]^m, \quad (1)$$

where B is the absorption coefficient, E_g is the optical band gap energy, h is Planck's constant, $\nu$is the frequency of incident photon, and m is an index which depends on the nature of electronic transition responsible for the optical absorption. Values of m for allowed direct and indirect transitions are 1/2 and 2, respectively. Optical transitions of the samples under study are indirect one. The indirect optical energy gap can be obtained from the intercept of the resulting linear region with the energy axis at $(\alpha h\nu)^2 = 0$. Figure 6 shows the Tauc's plot of the optical absorption spectrum measured at room temperature for calcium metaniobate nanopowder. Thus the determined band gap of calcium metaniobate is 3.25 eV. The absorption spectra indicate that the sample absorbs heavily in UV region and moderately in the visible region. Such materials find tremendous applications in UV filters and sensors.

3.5. Photoluminescence Study. The photoluminescence activity of the samples was investigated by recording the PL emission spectra of the as-prepared samples. The obtained PL spectra at the excitation wavelength of 350 nm are shown in Figure 7. The sample shows good luminescent property in the visible region. The transmission responsible for each emission is identified on the basis of the data by Payling and Larkins [22]. For $CaNb_2O_6$, the intense peak in the blue region at 442.5 nm corresponds to $3P_0^0 - 3D_1$ of Ca_I. The peak at 485.6 nm corresponds to $4S_{1.5}^0 - 4D_{1.5}$ transition of O_{II}. The peak at 528 nm is attributed to $3D_1 - 1P_1^0$ transition of Nb_I. The strong emission lines of the sample at specific wavelength make it useful in optoelectronic applications.

3.6. Sintering and Dielectric Properties. For the sintering behavior, the $CaNb_2O_6$ nanopowder was compressed as cylindrical discs and was sintered at 1350°C for 2 hours at a heating rate of 5°C/minute. The density of the sintered sample was calculated by "Archimedes" method and obtained >96%. The high density derived through the present study may be attributed to enhanced kinetics due to the small degree of agglomeration and ultrafine nature of the powder.

The SEM image of the sample given in Figure 8 shows the compactness of the sintered pellet. It is evident from the SEM that the sample achieved high densification with little porosity. From the SEM pattern, long rectangular sheet like patterns can be seen with their size in the micrometer range. Thus heat treatment resulted in grain growth up to several micrometers. The EDAX pattern shows that all the elements such as calcium, niobium, and oxygen are present in the sample in the same stoichiometric concentrations and are shown in Figure 9.

The dielectric constant ε_r and loss factor tanδ values of the sintered pellets were studied in the frequency range

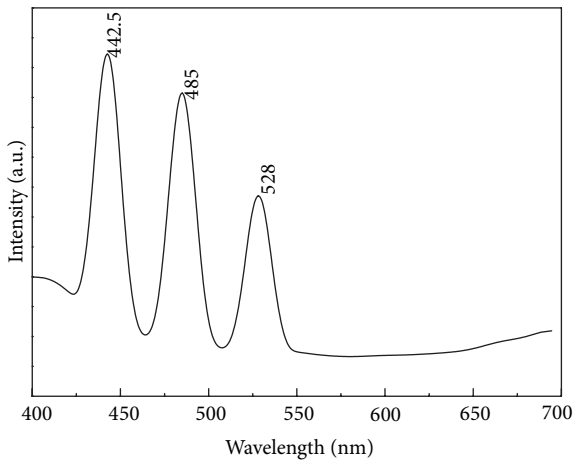

Figure 7: PL emission spectra of $CaNb_2O_6$.

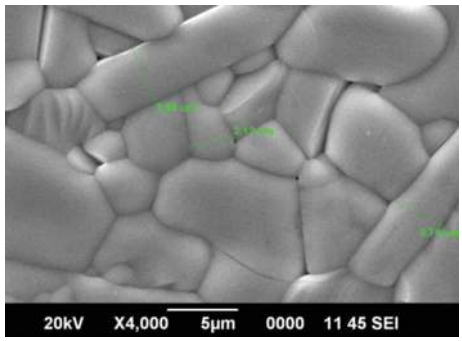

Figure 8: SEM micrograph of $CaNb_2O_6$.

100 Hz to 5 MHz at room temperature with silver electrodes on both sides of the circular disc. Figure 10 shows variation of ε_r and tanδ at room temperature with the frequency. The obtained dielectric constant ε_r and loss factor tanδ values of the $CaNb_2O_6$ pellets at 5 MHz were 27.6 and 5.3×10^{-4}, respectively. The values of dielectric constant and low loss factor indicate the suitability of the sample as a candidate for electronic and dielectric device applications.

4. Conclusions

Nanocrystalline semiconducting calcium metaniobate has been synthesized through an autoigniting combustion process. The X-ray diffraction study shows that the as-prepared nanopowder is single phase with orthorhombic structure. FT-Raman and FTIR studies showed that samples possess a distorted orthorhombic perovskite structure. TEM and SAED patterns confirm the nanocrystalline nature of the sample with an average particle size of 37 nm. The average optical band gap determined from Tauc's plot is 3.25 eV. PL measurements reveal that $CaNb_2O_6$ is a good photoluminar material. These nanocrystals were sintered at 1350°C to a high density in a short duration of 2 hours. The SEM image of the sintered sample indicates high densification of the material. The room temperature dielectric constant (ε_r) and loss factor

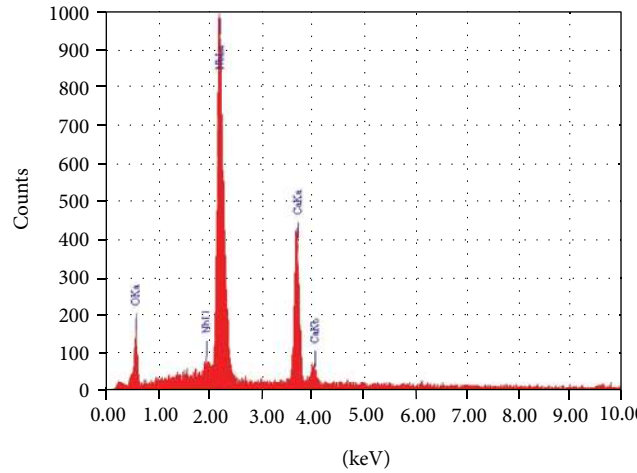

Figure 9: EDAX pattern of $CaNb_2O_6$.

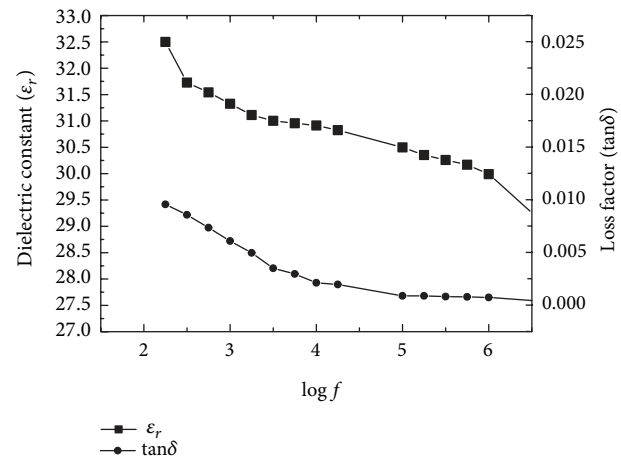

Figure 10: Variation of ε_r and tanδ with the frequency.

(tanδ) of the sintered pellet at 5 MHz are ~29 and 5.3×10^{-4}, respectively, which indicate that the material is suitable for electronic applications.

Conflict of Interests

The authors declare that there is no conflict of interests regarding the publication of this paper.

References

[1] J. P. Cummings and S. H. Simonsen, "The crystal structure of calcium niobate ($CaNb_2O_6$)," *American Mineralogist*, vol. 55, no. 1-2, pp. 90–97, 1970.

[2] R. C. Pullar, "The synthesis, properties, and applications of columbite niobates ($M^{2+}Nb_2O_6$): a critical review," *Journal of the American Ceramic Society*, vol. 92, p. 564, 2009.

[3] I. V. Kityk, M. Makowska-Janusik, M. D. Fontana, M. Aillerie, and F. Abdi, "Band structure treatment of the influence of nonstoichiometric defects on optical properties in $LiNbO_3$," *Journal of Applied Physics*, vol. 90, no. 11, pp. 5542–5549, 2001.

[4] H.-Z. An, C. Wang, T.-M. Wang, and W.-C. Hao, "Photocatalytic activity of M(M = Mg, Ca, Sr, Ba, Ni)Nb_2O_6," *Journal of Inorganic Materials*, vol. 22, no. 5, pp. 922–926, 2007.

[5] H. G. Kim, D. W. Hwang, S. W. Bae, J. Kim, V. R. Reddy, and K. H. Lee, "Synthesis and chacacterization of ANb_2O_6 (A = Ba, Ca, Co, Mg, Ni, Zn, Sr) photocatalysts," *Theories and Applications of Chemical Engineering*, vol. 8, p. 1, 2002.

[6] Y. Zhang, C. Liu, G. Pang et al., "Hydrothermal synthesis of a $CaNb_2O_6$ hierarchical micro/nanostructure and its enhanced photocatalytic activity," *European Journal of Inorganic Chemistry*, no. 8, pp. 1275–1282, 2010.

[7] I.-S. Cho, S. T. Bae, D. H. Kim, and K. S. Hong, "Effects of crystal and electronic structures of ANb_2O_6 (A = Ca, Sr, Ba) metaniobate compounds on their photocatalytic H_2 evolution from pure water," *International Journal of Hydrogen Energy*, vol. 35, no. 23, pp. 12954–12960, 2010.

[8] A. S. Bhalla, R. Guo, and R. Roy, "The perovskite structure—a review of its role in ceramic science and technology," *Materials Research Innovations*, vol. 4, no. 1, pp. 3–26, 2000.

[9] A. Wachtel, "Self-activated luminescence of M^{2+} niobates and tantalates," *Journal of the Electrochemical Society*, vol. 111, no. 5, pp. 534–538, 1964.

[10] A. A. Ballman, S. P. S. Porto, and A. Yariv, "Calcium niobate $Ca(NbO_3)_2$—a new laser host crystal," *Journal of Applied Physics*, vol. 34, no. 11, pp. 3155–3156, 1963.

[11] A. Yariv and J. P. Gordon, "The laser," *Proceedings of the IEEE*, vol. 51, no. 1, pp. 4–29, 1963.

[12] Y. Saito, H. Takao, T. Tani et al., "Lead-free piezoceramics," *Nature*, vol. 432, no. 7013, pp. 84–87, 2004.

[13] Y. Guo, K.-I. Kakimoto, and H. Ohsato, "Phase transitional behavior and piezoelectric properties of $(Na_{0.5}K_{0.5})NbO_3$-$LiNbO_3$ ceramics," *Applied Physics Letters*, vol. 85, no. 18, pp. 4121–4123, 2004.

[14] J. Satapathy and M. V. Ramanna Reddy, "Dielectric and thermal studies of ANb_2O_6 (A = Ca, Mg, Cu, Ni) for LTCC application," *International Journal of Applied Physics and Mathematics*, vol. 3, p. 181, 2011.

[15] H. J. Lee, K. S. Kong, and S. J. Kim, "Dielectric properties of MNB_2O_6 compounds (where M = Ca, Mn, Co, Ni, OR Zn)," *Materials Research Bulletin*, vol. 32, pp. 847–855, 1999.

[16] D.-W. Kim, H. B. Hong, K. S. Hong, C. K. Kim, and D. J. Kim, "The reversible phase transition and dielectric properties of $BaNb_2O_6$ polymorphs," *Japanese Journal of Applied Physics*, vol. 41, no. 10, pp. 6045–6048, 2002.

[17] Y.-J. Hsiao, C.-W. Liu, B.-T. Dai, and Y.-H. Chang, "Sol-gel synthesis and the luminescent properties of $CaNb_2O_6$ phosphor powders," *Journal of Alloys and Compounds*, vol. 475, no. 1-2, pp. 698–701, 2009.

[18] K. N. Singh and P. K. Bajpai, "Synthesis, structural, dielectric and electrical impedance study of $CaNb_2O_6$ phase pure material," *Journal of International Academy of Physical Sciences*, vol. 14, no. 4, pp. 501–510, 2010.

[19] K. C. Patil, "Advanced ceramics: combustion synthesis and properties," *Bulletin of Materials Science*, vol. 16, no. 6, pp. 533–541, 1993.

[20] E. Husson, Y. Repelin, N. Q. Dao, and H. Brusset, "Normal coordinate analysis for $CaNb_2O_6$ of columbite structure," *The Journal of Chemical Physics*, vol. 66, no. 11, pp. 5173–5180, 1977.

[21] F. D. Hardcastle and I. E. Wachs, "Determination of niobium-oxygen bond distances and bond orders by Raman spectroscopy," *Solid State Ionics*, vol. 45, no. 3-4, pp. 201–213, 1991.

[22] R. Payling and P. Larkins, *Optical Emission Line of Elements*, John Wiley & Sons, New York, NY, USA, 1st edition, 2000.